Microstructure and Properties of Cast Ingots of Al-Zn-Mg-Cu Alloys Modified with Sc and Zr*

O.N. Senkov[1**], R.B. Bhat[1], S.V. Senkova[1], and D. Schloz[2]

[1]UES Inc., 4401 Dayton-Xenia Road, Dayton, Ohio 45432-1894, USA

[2]Wagstaff, Inc., 3910 North Florida Road, Spokane, WA 99216-1720, USA

ABSTRACT

The effect of combined additions of Sc and Zr on the microstructure and tensile properties of the direct chill (DC) cast ingots of developmental Al-Zn-Mg-Cu alloys has been evaluated in this work. The properties in both the longitudinal and transverse directions of the cast ingots were determined in as-cast and cast plus heat-treated conditions, at room and cryogenic temperatures. Extensive microstructural evaluation was carried out using optical and electron microscopy, including orientation image microscopy by the electron backscatter diffraction technique. The Sc-containing developmental cast alloys showed the tensile properties, which are much better than the properties of any commercial cast Al alloys and are similar or even superior to the properties of 7075-T6 alloy forgings. The microstructural evolution, the strengthening mechanisms, optimum content of the dispersoid-forming elements, and the processing-structure-property correlations are discussed.

1 INTRODUCTION

High-strength Al-Zn-Mg-Cu (7XXX series) alloys are extensively used in the aerospace industry, where newer materials with high specific properties are always in high demand. Their strength is mainly controlled by the aging process of precipitation and growth of very fine precipitates of the η′ phase (a semi-coherent, metastable form of the equilibrium $MgZn_2$ phase), which is enriched with zinc and magnesium; and the effect of copper is to increase the aging rate by increasing the degree of super-saturation and, possibly, through nucleation of $CuMgAl_2$ (S-

* Approved for public release; distribution unlimited.

** Corresponding author. Telephone: 937-2551320; Fax: 937-656-7292; E-mail: oleg.senkov@wpafb.af.mil.

Report Documentation Page

Form Approved
OMB No. 0704-0188

1. REPORT DATE	2. REPORT TYPE	3. DATES COVERED
OCT 2004		**-**

4. TITLE AND SUBTITLE	5a. CONTRACT NUMBER
Microstructure and Properties of Cast Ingots of AL-ZN-Mg-Cu Alloys Modified with Sc and Zr	**F04611-02-C-0014**
	5b. GRANT NUMBER
	5c. PROGRAM ELEMENT NUMBER

6. AUTHOR(S)	5d. PROJECT NUMBER
Oleg Senkov; R Bhat; S Senkova; D Schloz	**3005**
	5e. TASK NUMBER **02AF**
	5f. WORK UNIT NUMBER

7. PERFORMING ORGANIZATION NAME(S) AND ADDRESS(ES)	8. PERFORMING ORGANIZATION REPORT NUMBER
UES, Inc.,4401 Dayton-Xenia Road,Dayton,OH,45432-1894	

9. SPONSORING/MONITORING AGENCY NAME(S) AND ADDRESS(ES)	10. SPONSOR/MONITOR'S ACRONYM(S)
	11. SPONSOR/MONITOR'S REPORT NUMBER(S)

12. DISTRIBUTION/AVAILABILITY STATEMENT

Approved for public release; distribution unlimited

13. SUPPLEMENTARY NOTES

14. ABSTRACT

The effect of combined additions of Sc and Zr on the microstructure and tensile properties of the direct chill (DC) cast ingots of developmental Al-Zn-Mg-Cu alloys has been evaluated in this work. The properties in both the longitudinal and transverse directions of the cast ingots were determined in as-cast and cast plus heat-treated conditions, at room and cryogenic temperatures. Extensive microstructural evaluation was carried out using optical and electron microscopy, including orientation image microscopy by the electron backscatter diffraction technique. The Sc-containing developmental cast alloys showed the tensile properties, which are much better than the properties of any commercial cast Al alloys and are similar or even superior to the properties of 7075-T6 alloy forgings. The microstructural evolution, the strengthening mechanisms, optimum content of the dispersoid-forming elements, and the processing-structure-property correlations are discussed.

15. SUBJECT TERMS

16. SECURITY CLASSIFICATION OF:			17. LIMITATION OF ABSTRACT	18. NUMBER OF PAGES	19a. NAME OF RESPONSIBLE PERSON
a. REPORT	b. ABSTRACT	c. THIS PAGE			
unclassified	**unclassified**	**unclassified**		**24**	

phase). [1,2] The strengths of these alloys generally increase with the concentrations of Zn and Mg; however the alloys become prone to hot cracking during casting or during rapid cooling from a processing temperature when the amount of Zn exceeds 7-8%. Fortunately, the fracture-related properties of these alloys can considerably be improved by small additions of Sc [3-5], which enables superior combination of higher strength levels and acceptable ductility [6-8].

The effect of scandium additions to advanced aluminum alloys has been studied extensively [9-11] and synergistic advantages are known to accrue when scandium is added together with zirconium [12]. In addition to refining the grain size of the Al alloys during casting, Sc and Zr additions also increase the resistance to recrystallization during hot working and contribute to further strengthening by the formation of fine coherent $Al_3(Sc,Zr)$ dispersoids [13-17]. Accordingly, the maximum benefit from Sc and Zr additions is obtained by producing a supersaturated solid solution of these elements during casting, which is then decomposed to produce a high number density of fine $Al_3(Sc,Zr)$ dispersoids during controlled heat treatment . The uniform distribution of these dispersoids also promotes the formation of a stable refined subgrain structure during thermomechanical processing, which results in further strength enhancement.

In spite of a number of publications devoted to the effect of Sc and Zr on the mechanical properties of 7XXX series alloys in wrought condition, no results are yet available in the open literature on the effect of these elements on the mechanical properties of the 7XXX series alloys in the as-cast condition. One may however expect considerable improvements in the mechanical properties due to the refining effect from the Sc addition and additional strengthening from fine $Al_3(Sc,Zr)$ dispersoids following heat treatment. The purpose of the present work was to examine the potential beneficial effects of combined additions of Sc and Zr on microstructure and tensile properties of an Al-Zn-Mg-Cu alloy in as-cast condition. The work also covers the effects of homogenization and heat treatment on the tensile properties of these castings.

2 EXPERIMENTAL

Four Sc-modified 7XXX series alloys having the compositions shown in Table 1 were produced by continuous direct chill (DC) casting at Wagstaff, Inc., Spokane, WA. The cast ingots were 76 mm in diameter and about 4000 mm in length, and they all had the same nominal composition, including ~0.17% Zr and up to 0.6% of other dispersoid forming elements such as Mn, Cr, Fe and Si, but

different Sc concentrations of 0%, 0.18%, 0.38% and 0.48% Sc (all compositions are in weight percent). These alloys were developed by UES, Inc., Dayton, Ohio under the U.S. Air Force contract F04611-01-C-0030 (pending U.S. patents, applications No. 10/291,184 and 10/291,201). The microstructure and tensile properties of the alloys were studied in as-cast and heat-treated conditions. An optical microscope Reichterjung and a scanning electron microscope (SEM) LEICA 360FE were used for microstructural analysis. SEM backscatter electron (BSE) analysis was conducted on polished specimens, while optical microscopy was carried out on specimens, which were initially polished and then etched using an etching solution (5 ml HF, 20 ml HNO_3, and 75 ml H_2O). In addition, electrolytically polished specimens were studied by orientation image microscopy (OIM) using an electron backscatter diffraction (EBSD) technique in the SEM equipped with TexSEM Laboratories Inc., (TSL) OIM data collection and analysis software (version 3.5). Tensile specimens were machined from cast ingot sections located about 15-20 mm away from the surface of the ingots, at both longitudinal and transverse orientations. The longitudinal direction was parallel to the ingot axis, and the transverse direction was perpendicular to the radial direction in the transverse cross-section of the ingot. The specimen gauge had a rectangular cross section of 3.6 mm x 2.5 mm and a length of 20 mm. Some specimens were heat treated in air using resistance heated muffle furnaces. Heat treatment used in this study consisted of homogenization annealing at 460ºC for 48 hours, water quenching and artificial aging (120ºC for 19 hours); this heat treatment is further referred to as H+T6. The tensile tests were conducted at room temperature (RT, 25ºC) and a cryogenic temperature (CT, -196ºC) using a servo-hydraulic MTS testing machine and a constant ram speed of 0.02 mm/s (initial strain rate is 10^{-3} s^{-1}). The fracture surfaces of the tensile tested specimens were examined using SEM in a secondary electron diffraction mode.

3 RESULTS AND DISCUSSION

3.1 Microstructure

Macro etching of the transverse cross-sections of the DC cast ingots revealed that the alloy without Sc (SSA000) had a non-homogeneous, feathery grain structure, with grains of several millimeters in size growing from the surface of the ingot to the center (Figure 1a). Shrinkage-induced, pre-solidification cracks were also detected in the central part of this ingot. Other three alloys, which

additionally contained Sc, had a very homogeneous equiaxed grain structure, and no cracks or macro-porosity were detected (Figures 1b and 1c).

Figures 2 to 5 show BSE images of the longitudinal and transverse cross sections of the alloys containing different amounts of Sc. Although the dendritic structure is present after casting in both Sc-free and Sc-bearing alloys, the morphology and sizes of the dendrites are different. The photomicrographs from the Sc-free SSA000 alloy clearly reveal columnar twinned dendrites with the dendritic trunks slightly (about 10 degrees) inclined to the longitudinal direction of the cast ingot (the longitudinal direction is vertical in Figures 2a, 3a, 4a, and 5a). EBSD analysis shows that the dendrite trunks and secondary arms in this alloy grow in <110> directions (Figure 6), which is typical for solidification conditions leading to the feathery grain structure [18-21]. With an increase in the Sc content, the primary dendrite arms (trunks) become shorter, their columnar (directional) arrangement transforms to a random arrangement, the preferential growth directions switch to <100>, and a completely equiaxed grain structure is formed in the alloys with 0.38% Sc and 0.48% Sc, see Figures 3, 4 and 5. The grain size decreases with an increase in the concentration of Sc from ~120 μm for the alloy SSA018 to 100 μm for SSA038 and to 80 μm for SSA048. The X-ray energy dispersive spectrometry (XEDS) showed that the inter-dendritic regions (they have a bright color in the BSE images of Figures 2 to 5) are enriched with Zn, Mg and Cu (about 14 at.% Zn, 14 at. % Mg, and 7 at.% Cu), and the gray-color dendritic arms are enriched with Al, depleted with Zn, Mg, and Cu, and contain traces of Mn, Zr, and Sc (each of them is ~0.05-0.1 at.% or less). An additional feature typical to the alloys SSA038 and SSA048, is the presence of the primary $Al_3(Sc,Zr)$ particles in the center of almost every dendrite grain (Figures 4 and 5), which indicates that these particles must have been the first to nucleate and grow in the molten aluminum and to contribute to the nucleation of the aluminum dendrites, either directly or indirectly. On the other hand, in the alloy SSA018, which also exhibits considerable grain refinement relative to the Sc-free alloy SSA000, the primary $Al_3(Sc,Zr)$ particles were detected only inside a few grains.

After homogenization, most of the Zn-, Mg-, and Cu-rich intermetallic phases at the cell and secondary dendrite arm boundaries dissolve, and these boundaries become less identifiable. In the alloy SSA000 with no Sc, a series of parallel lamellae of alternating orientations are formed inside the large feathery grains (see Figure 6a). These lamellae are successively separated by straight and wavy boundaries, which are white-colored in Figure 6a. The pole figures from these lamellae (Figure 6b) obtained from EBSD/OIM analysis show the twin relationship between these lamellae, with

a 60º rotation about the [111] crystal direction. In particular, the orientation relationships $[001]_M$ || $[22\bar{1}]_T$ and $[22\bar{1}]_M$ || $[001]_T$ are clearly identified from (001) and (221) pole figures in Figure 6b. The fraction of the twin boundaries is rather high, about 63%, and the misorientation angle distribution between the adjacent grains has a sharp maximum at 60 degrees (Figure 6c). The twin thickness in the homogenized alloy is about 25 μm (Figure 6a), which is about half of the dendrite thickness in the as-cast alloy (Figure 2). Similar twinned columnar (also sometimes referred to as feathery) grain structure has been observed in a number of Al- based alloys directly solidified under high thermal gradient and cooling rate without grain refiners [18-21]. These morphology features have been explained by twin formation in <110> growing dendrites and twinned orientations of the dendrites in each feathery grain [19-21]. These coherent twin boundaries most likely accelerate the growth rate of the twinned dendrite arms by producing sharp front tips [24]. The coherent twin boundaries formed inside the primary arms (trunks) remain straight, while the interfaces between the secondary arms of the nearest dendrites create serrated incoherent twin boundaries after homogenizing annealing.

It should be noticed that the twinned columnar grain microstructure is generally observed in aluminum alloy ingots, which are cast without grain refiners [2, p.524]. In the present work, however, the alloy SSA000 contained rather large amount (0.17%) of Zr, which is considered as a strong grain-refining element for 7XXX series alloys [1,2]. Ineffectiveness of Zr for grain refinement in the present work may be explained by high superheat of the molten alloy, as the casting was conducted from the temperature of ~780ºC, and high thermal gradients are known to promote twinned columnar grain growth [22]. It is recognized that due to the high superheat required to cast Zr-containing Al alloys, such as 2219 and 7050, these alloys are prone to the formation of twinned columnar grains during casting [26].

An equiaxed grain structure is formed in the alloys containing Sc after homogenization and no twins are identified (see Figures 7 and 8). The average grain size, according to OIM, is around 120 μm for the alloy SSA018 and 80 μm for SSA048; these values are similar to the as-cast condition, which indicates that no grain growth occurred during the homogenizing annealing. The discrete pole figures and the distributions of the misorientation angles between the adjacent grains confirm random orientations of grains in these alloys. For example, in Figure 7b a (011) discrete pole figure from the transverse cross-section of the cast and homogenized alloy SSA018

is given. The black dots, which represent the <011> directions from every individual grain, are evenly distributed in this pole figure due to the random orientation of the grains.

The synergistic grain refining effect from Sc and Zr added together has been reported in a number of publications (see, for example [4-11]) and it has been explained by the presence of primary $Al_3(Sc,Zr)$ particles, which solidify first and contribute to crystallization in these alloys. Indeed, the microstructural analysis conducted in this work shows that a number of the equiaxed dendrites in the alloys with 0.38% Sc and 0.48% Sc nucleate on the primary $Al_3(Sc,Zr)$ particles. However, considerable grain refinement is also observed in the alloy with 0.18% Sc. In this alloy, only a few primary $Al_3(Sc,Zr)$ particles were detected, which could not be responsible for the grain refinement; therefore, other grain refining mechanisms from the Sc addition should also be considered. A considerable decrease in the fraction of twin boundaries with the Sc addition may suggest that Sc increases the anisotropy of the surface tension of the solid-liquid interface and prevents formation of twinned <110> dendrite arms. Instead, untwinned <100> arms with slower growth kinetics are formed [19,23]. Another possibility (which however should be experimentally proven) is that Sc increases the solid-liquid surface energy. This should decrease the constitutional super-cooling, slow down the rate of the dendrite growth, accelerate dissolution and separation of the dendrite arms, and, therefore, accelerate grain multiplication during solidification [19,24].

3.2 Mechanical Properties

Properties in as-cast condition.

Room temperature (RT) and cryogenic temperature (CT) tensile properties of the as-cast alloys after about one year holding at room temperature are given in Table 2. The alloy SSA000, without Sc, showed very anisotropic properties. For example, the RT tensile strength was 378 MPa and the plastic strain (El) was 15% in the longitudinal direction, however, only 318 MPa and 0.01% in the transverse direction. Both yield strength (YS) and ultimate tensile strength (UTS) increase with a decrease in the temperature, and at T = –196ºC, YS = 357 MPa and UTS=439 MPa for SSA000 in the longitudinal direction. The transverse properties of the cast alloy SSA000 can be compared with the properties of a commercial as-cast 7050Al alloy ingot reported by Wan et al. [25] The ingot had dimensions of 1370 mm width and 406 mm thickness, and the tensile strength varied from 325 MPa near the surface to 250 MPa near the center of the

ingot, with nil elongation. The orientation of the specimens with reference to the casting direction was not reported in [25]; however from the nil elongation values, the transverse orientation may be assumed. The different strength values were correlated with the different cooling rate along the ingot thickness. The cooling rate decreases from the surface to the center of the ingot, resulting in an increase in the grain size and the volume fraction of the inter-dendritic phases; both factors reduce the strength [25]. The effect of twinned columnar grains on the mechanical properties of 7050 Al alloy has been studied in detail and the highly anisotropic properties attributed to the preferred fracture along the twin planes as well as the higher segregation of solute elements found on those fracture surfaces [26]. It is evident that the twinned columnar grain structure of this alloy is responsible for such anisotropic behavior. The addition of Sc improves both the yield and ultimate tensile strengths of the as cast alloys, the increase being higher for larger Sc additions (Table 2). The increase in the Sc concentration up to 0.48% leads to an increase in the tensile strength by about 14 MPa for each 0.1%Sc added. For example, the alloy SSA048 shows YS = 317-324 MPa, UTS = 425-433 MPa and El=3-4% at room temperature. None of the currently available commercial Al alloys has such superior combination of the tensile properties in as-cast condition [27]. The deformation-induced strengthening is also higher in the Sc containing alloys (Table 4). For example, in as-cast alloys the strength increase per every 1% of the plastic strain was ~8-9 MPa in the alloy without Sc and ~20-35 MPa in the alloys containing Sc. The improvement in yield strength and the work hardening in the as cast condition is due to a combined effect of grain refinement as well as solid solution, precursors to dispersoids, and dispersoids strengthening. The ductility in the longitudinal direction is lower in the Sc containing alloys, but the same is higher in the transverse direction as compared to the alloy without Sc. This effect remarkably improves the isotropy of the cast alloys with Sc and it is mainly due to the change in grain morphology and the grain orientation due to Sc addition, discussed earlier. In all four developmental alloys, a decrease in the temperature of testing from 25ºC to –196ºC led to an increase in YS by ~100 MPa and UTS by ~50-60 MPa and about 50% decrease in the tensile ductility.

Properties in homogenized and T6-tempered condition.

The tensile properties of the alloys after homogenization and T6 tempering (H+T6 condition) are given in Table 3. The tensile strength in the longitudinal direction of the alloy SSA000 increases

considerably (by about 40%) and the ductility does not change after the heat treatment. However, the tensile strength does not improve and the alloy still shows brittle behavior in the transverse direction, so that the anisotropy of the alloy increases after the heat treatment. In the Sc-containing alloys, on the other hand, the tensile strength and ductility increase in both longitudinal and transverse directions, and these alloys have isotropic properties after the heat treatment. For example, the alloy SSA038 has a minimum YS=494 MPa, UTS=593 MPA and El=13% at room temperature and YS=603 MPa, UTS=700 MPa and El=6% at the cryogenic temperature. These tensile properties of the developmental Sc-containing alloys in *cast-and-heat-treated* condition are similar to the properties of the best commercial 7XXX series alloys in *wrought-and-heat-treated* (e.g. forged) condition [27]. For example at RT, 7075-T6 die forgings have YS=485 MPa, UTS=550 MPA and El=14% [27].

Homogenization of the cast ingots is normally carried out to mitigate the effects of micro- and macro-segregation, by allowing time at high temperatures to dissolve the Zn-, Mg-, and Cu- rich intermetallic phases and to achieve a uniform composition throughout the ingot. In the Sc-containing alloys, homogenization may also result in the precipitation and subsequent growth of secondary $Al_3(Sc,Zr)$ dispersoids from the supersaturated solid solution of Sc and Zr [28,29]; the latter is formed during rapid DC casting. After homogenization, the aluminum matrix becomes enriched with Zn, Mg, and Cu and depleted with other elements that form non-soluble dispersoids. Consecutive aging leads to decomposition of the supersaturated solid solution and fine precipitation of the η' phase [1,2]. As a result, the strength of the Sc-containing alloys is a combined effect of the dispersoid, precipitation, solid solution, and grain boundary strengthening [30].

The increase in the yield strength of the heat-treated developmental alloys, as compared to the as-cast condition, almost does not depend on the amount of Sc and, therefore, it is mainly due to precipitation of η' particles during aging. For example, YS increased by ~180 MPa at room temperature and by ~190 MPa at the cryogenic temperature for all four alloys after the heat treatment (Compare Tables 2 and 3). On the other hand, the deformation-induced strengthening is higher in the Sc containing alloys, and its magnitude decreases after heat treatment (Table 4). For example, in as-cast alloys the strength increase per every 1% of the plastic strain was ~8-9 MPa in the alloy without Sc and ~20-35 MPa in the alloys containing Sc; while after heat treatment, these values decreased to to about ~5-8 MPa in the alloy without Sc and to ~7-15 MPa in the alloys with Sc (Table 4). Since the heat treatment does not lead to any significant grain growth, the stronger strain-induced strengthening effect in the as-cast Sc

containing alloys is definitely due to more intense dislocation multiplication in the presence of Sc in the solid solution. The dislocation annihilation is restricted because of the pinning effect. Homogenizing treatment reduces the amount of Sc in the solid solution by formation of fine $Al_3(Sc,Zr)$ dispersoids; this allows dislocations to annihilate more easily during deformation.

Homogenization treatment also improves the ductility in the Sc containing alloys. The ductility is controlled by the brittle intermetallic precipitates (bright phase in Figure 9a) existing in the interdendritic regions, especially in the Sc containing alloys, which have equiaxed grain morphology. Homogenization treatment results in the dissolution of these precipitates as can be seen from the Figure 9b, and the consequent improvement in ductility. In the alloy without Sc, however, the ductility is controlled by the twinned columnar grain morphology and the orientation of the grains with respect to the specimen testing direction [26]. The homogenization treatment has no effect on both grain morphology as well as the orientation and as such ductility is not affected by the heat treatment in the alloy without Sc (SSA000).

The results presented in Tables 2 and 3 also show that an increase in the Sc content beyond 0.38% has almost no advantage on tensile properties and even leads to a decrease in ductility. This can be explained by the presence of brittle coarse $Al_3(Sc,Zr)$ particles in the alloys with high Sc content (see below). These particles add not much to strength; however, their presence can limit the volume fraction of fine secondary $Al_3(Sc,Zr)$ dispersoids responsible for additional strengthening of these alloys and as well as participate in the initiation of fracture.

3.3 Fractography

SEM images of fracture surfaces, which are typical to the tensile specimens of the alloys with and without Sc, are presented in Figure 10. On the microscopic level, all the specimens showed dimple, ductile type fracture. The alloy without Sc (SSA000) after deformation in the longitudinal direction have trans-granular fracture with evenly distributed dimples of different sizes, which are initiated by cleaved intermetallic particles (Figure 10a). The fracture surface morphology becomes completely different when this alloy is deformed in the transverse direction. For this orientation, columnar grain features and fracture along the feathery grain boundaries can be clearly identified (Figure 10b). This further confirms the conclusion that ductility in the alloy without scandium is determined by the highly anisotropic nature of the

twinned columnar grain morphology and the orientation of the test specimen with reference to the stress axis.

The alloys containing Sc have mixed trans-granular and inter-granular ductile dimple fracture showing the presence of equiaxed grains in both longitudinal and transverse cross-sections (Figures 10c and 10d). Similar to the Sc-free alloy in the longitudinal orientation, the dimples are initiated by cleaved intermetallic particles. Figure 10 shows a coarse primary $Al_3(Sc,Zr)$ particle appearing on the fracture surface of the alloy SSA048. This particle has a flat surface formed during the brittle cleavage fracture and it is located in the bottom of a deep hole, which was formed during extensive plastic deformation of the surrounding ductile matrix. These brittle coarse primary $Al_3(Sc,Zr)$ particles slightly decrease ductility of the SSA048, relative to the ductility of the alloy SSA038, which has a smaller Sc content.

4 SUMMARY AND CONCLUSIONS

Microstructure and mechanical properties of a 7XXX series alloy modified with Zr and different levels of Sc, produced by the DC casting route have been evaluated in the as cast and heat treated conditions. The following conclusions can be drawn from this study:

a) Additions of Sc provide considerable grain refinement and inhibit formation of twinned columnar grains and cracks in casting. An addition of 0.18%Sc could suppress the formation of solidification cracks and reduce the grain size to about 120 μm.

b) Higher scandium contents of 0.38% and 0.48% however lead to the formation of coarse primary Al_3 (Sc, Zr) particles, which are also brittle and consequent deterioration of mechanical properties.

c) Scandium additions also resulted in an isotropic material due to the equiaxed grain morphology resulting from the change in the growth orientation.

d)Homogenization and T6 treatment improved both the strength and elongation of Sc-containing alloys.

e) Typical yield strength of 490 MPa, UTS of 590 MPa and 15% elongation at room temperature and yield strength of 610 MPa, UTS of 720 MPa and 10% elongation at liquid nitrogen temperature have been achieved in the cast and heat treated condition in an alloy modified with 0.38% scandium. These values exceed the properties achieved in wrought 7075-T6 alloy. Further improvement is expected by the optimization of homogenization being carried out.

5 ACKNOWLEDGEMENTS

The authors would like to thank Drs. Daniel Miracle and Kevin Kendig, Air Force Research Laboratory, Wright-Patterson AFB, OH, Dr. Madan Mendiratta, UES Inc., OH, and Professor Roger Doherty, Drexel University, PA, for useful technical discussions. The work was financially supported through the US Air Force SBIR contract No. F04611-02-C-0014 (Dr. Jeigh Shelly, Program Manager).

6 REFERENCES

1. J.E. Hatch (Ed.), *Aluminum: Properties and Physical Metallurgy*, ASM International, Materials Park, OH, USA, 1984.
2. J.R. Davis (Ed.), *Aluminum and Aluminum Alloys (ASM Specialty Handbook),* ASM International, Materials Park, OH, 1993.
3. V.I. Elagin, *Technology of Light Alloys (Tekhnologiya Legkikh Splavov, USSR)*, No. 9 (1989) 5-14.
4. V.I. Elagin, V.V. Zakharov, T.D. Rostova, *Metal Science and Heat Treatment*, Vol. 36, No. 7-8, (1995) 375-380.
5. R.R. Sawtell, and C.L. Jensen, *Metal. Trans. A,* 21A, (1990), 421-430.
6. O.N. Senkov, R.B. Bhat, and S.V. Senkova, in: *Metallic Materials with High Structural Efficiency, O.N. Senkov, D.B. Miracle, S.A. Firstov, Eds*, (Kluwer Acad. Publishers, Dordrecht, The Netherlands, 2004) pp. 151-162.
7. O.N. Senkov, D.B. Miracle, Y.V. Milman, J.M. Scott, D.V. Lotsko, A.I. Sirko, *Mater. Sci. Forum*, 396-402 (2002) 1127-1132.
8. Y.V. Milman, A.I. Sirko, D.V. Lotsko, D.B. Miracle, O.N. Senkov, *Mater. Sci. Forum,* 396-402 (2002) 1217-1222.
9. L.S. Toporova, D.G. Eskin, M.L. Kharakterova, and T.V. Dobatkina (Eds.), *Advanced Aluminum Alloys Containing Scandium-Structure and Properties*, Gordon and Breach Science Publishers, The Netherlands, 1998.
10. A.K. Mukhopadhyay, G.M. Reddy, K.S. Prasad, S.V. Kamat, A. Dutta, and C. Mondal, in: *Advances in the Metallurgy of Al Alloys*, Proceedings of the J.T.Staley Honorary Symposium on Aluminum Alloys, (ASM International, Materials Park, OH, 2001) pp.63-71

11. V. Singh, K.S. Prasad, and A. Gokhale, *Scripta Materialia*, 50 (2004) 903-908
12. Y.W. Riddle and T.H. Sanders Jr., *Materials Science Forum*, 331-337 (2000) 799-804.
13. T.D. Rostova, V.G. Davydov, V.I. Yelagin, and V.V. Zakharov, *Materials Science Forum,* 331-337 (2000) 793-798.
14. F.A. Costello, J.D. Robson and P.B. Prangnell, *Mater. Sci. Forum,* 396-402 (2002) 757-762.
15. J.D. Robson and P.B. Prangnell, *Mater. Sci. Technol.*, 18 (2002) 607.
16. B. Morere, C. Maurice, R. Shahani, and J. Driver, *Met.Mater.Trans.A.,* 32A (2001) 625.
17. Y.W. Riddle and T.H. Sanders Jr., *Materials Science Forum*, 331-337 (2000) 939-944
18. V.O. Esin, I.G. Brodova, G.N. Pankin, I.P. Korshunov, *Fiz. Met. Metalloved*., 50, No. 4 (1980) 886-889.
19. S. Henry and M. Rappaz, *Mater. Sci. Forum*, 329-330 (2000) 65-72.
20. S. Henry, P. Jarry, and M. Rappaz, *Metall. Mater. Trans. A*, 29A (1998) 2807-2817.
21. S. Henry, T. Minghetti, and M. Rappaz, *Acta Materialia*, 46 (1998) 6431-6443.
22. R.E. Spear, R.T. Craig, and C.R. Howle, *J. of Metals,* 23, No. 10 (1971) 42-45.
23. M.C. Flemings, *Solidification Processing*, McGraw-Hill, New York, 1974.
24. W. Kurz and D.J. Fisher, *Fundamentals of Solidification*, Trans. Tech. Publications, Switzerland, 1984
25. J. Wan, H.M. Lu, K.M. Chang, and J. Harris, in: Barry Welch (Ed.), *Light Metals,* (TMS, Warrendale, PA, 1998) pp.1065-1070.
26. D.A.Granger and J.Liu, *J.of Metals,* 35, No.6 (1983) 54-59.
27. J.G. Kaufman, Properties of Aluminum Alloys: Tensile, Creep, and Fatigue Data at High and Low Temperatures (ASM International, Materials Park, OH, 1999).
28. J.D. Robson and P.B.Prangnell, *Acta Materialia,* 49 (2001) 599-613
29. J.D. Robson, *Acta Materialia,* 52 (2004) 1409-1421
30. K.L. Kendig and D.B. Miracle, *Acta Materialia*, 50 (2001) 4165-4175.

FIGURE CAPTIONS

Figure 1. Photographs of etched transverse cross-sections of DC cast ingots of alloys (a) SSA000, (b) SSA018 and (c) SSA048. The diameter of the ingots is 76 mm.

Figure 2. SEM backscatter micrographs of (a) longitudinal and (b) transverse cross-sections of the DC cast ingot of alloy SSA000.

Figure 3. SEM backscatter micrographs of (a) longitudinal and (b) transverse cross-sections of the DC cast ingot of alloy SSA018.

Figure 4. SEM backscatter micrographs of (a) longitudinal and (b) transverse cross-sections of the DC cast ingot of alloy SSA038.

Figure 5. SEM backscatter micrographs of (a) longitudinal and (b) transverse cross-sections of the DC cast ingot of alloy SSA048.

Figure 6. Orientation imaging microscopy (OIM) data of alloy SSA000 showing (a) the grain structure, (b) characteristic pole figures and (c) the misorientation angle distribution between the adjacent grains. In figure (a), the boundaries between the matrix and twins are highlighted with white lines, and the boundaries between the matrix grains are highlighted with black lines. In figure (b) <221> poles from twins and the matrix, which are parallel to <001> poles from the matrix and twins, respectively, are circled.

Figure 7. Orientation imaging microscopy (OIM) data of alloy SSA018 showing (a) the grain structure, (b) the (011) discrete pole figure showing orientations of all individual grains, (c) the grain size distribution plot and (d) the distribution of the misorientation angle between the adjacent grains.

Figure 8. Orientation imaging microscopy (OIM) data of alloy SSA048 showing (a) the grain structure, (b) the grain size distribution plot and (c) the distribution of the misorientation angle between the adjacent grains.

Figure 9. SEM BSE micrographs of SSA018 showing (a) as-cast and (b) as-homogenized structure.

Figure 10. SEM fractographs of tensile specimens of the alloys SSA000 (a and b) and SSA018 (c and d), with the tensile axis in the longitudinal (a, c) and transverse (b, d) directions. H+T6 condition, room temperature deformation.

Figure 11. SEM fractograph from the alloy SSA048 showing cleavage fracture of a coarse primary $Al_3(Sc,Zr)$ particle.

Tables

Table 1. Composition (wt.%) of alloys used in this work.

Alloy ID	Zn	Mg	Cu	Mn	Zr	Sc	Others	Al
SSA000	7.14	2.30	1.61	0.27	0.17	0	up to 0.3	Bal.
SSA018	7.17	2.20	1.58	0.30	0.18	0.18	up to 0.3	Bal.
SSA038	7.11	2.14	1.56	0.25	0.17	0.38	up to 0.3	Bal.
SSA048	7.05	2.35	1.55	0.27	0.14	0.49	up to 0.3	Bal.

Table 2. Room temperature (RT) and cryogenic temperature (CT) tensile properties of four as-cast developmental alloys in longitudinal/transverse directions.

Temperature	25ºC			-196ºC		
Property	YS (MPa)	UTS (MPa)	El (%)	YS (MPa)	UTS (MPa)	El (%)
SSA000	257/318	378/318	15/0.01	357/377	439/377	9/0.01
SSA018	292/284	402/379	5/3	395/368	462/415	2/1
SSA038	313/305	445/409	8/3	406/411	495/481	4/2
SSA048	324/317	433/425	4/3	422/421	504/478	2/1

Table 3. RT and CT tensile properties of cast and H+T6 heat-treated developmental alloys in longitudinal/transverse directions.

Temperature	25ºC			-196ºC		
Property	YS (MPa)	UTS (MPa)	El (%)	YS (MPa)	UTS (MPa)	El (%)
SSA000	439/304	520/304	15/0.01	528/384	607/384	9/0.01
SSA018	457/452	552/559	14/11	584/570	674/679	10/7
SSA038	494/497	593/595	15/13	610/603	719/700	10/6
SSA048	505/508	600/600	12/9	613/624	717/709	8/7

Table 4. An average increment in strength per every percent of the plastic strain increase in as–cast and cast plus heat-treated developmental alloys at room and cryogenic temperatures. The values are given in MPa/pct.

Temperature	25ºC		-196ºC	
Alloy/Condition	As-cast	Cast+H+T6	As-cast	Cast+H+T6
SSA000	8	5	9	9
SSA018	27	8	33	12
SSA038	26	7	29	13
SSA048	31	9	42	12

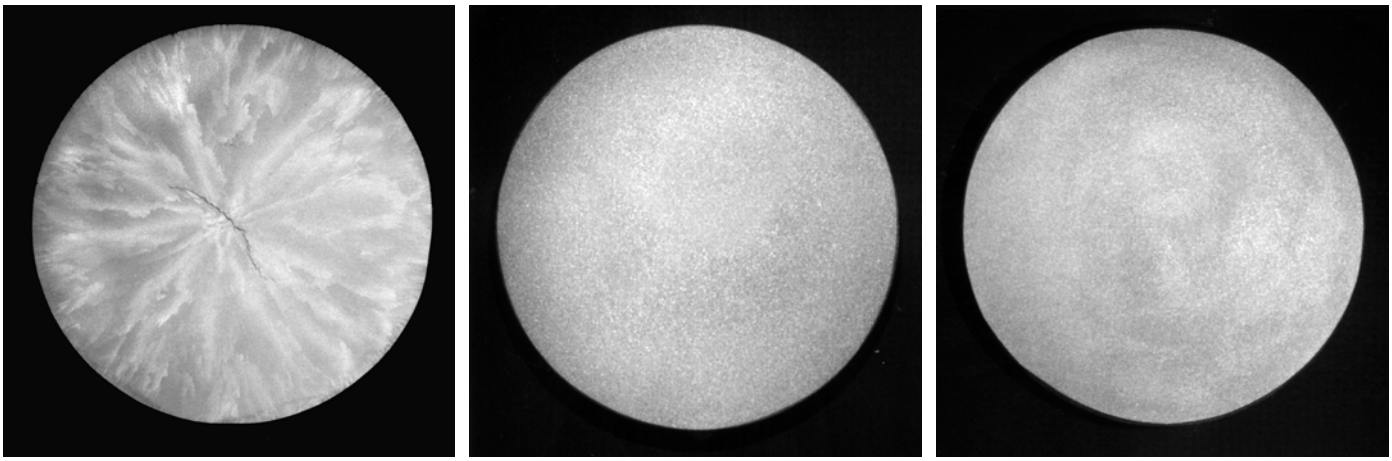

(a) (b) (c)

Figure 1.Photographs of etched transverse cross-sections of DC cast ingots of alloys (a) SSA000, (b) SSA018 and (c) SSA048. The diameter of the ingots is 76 mm.

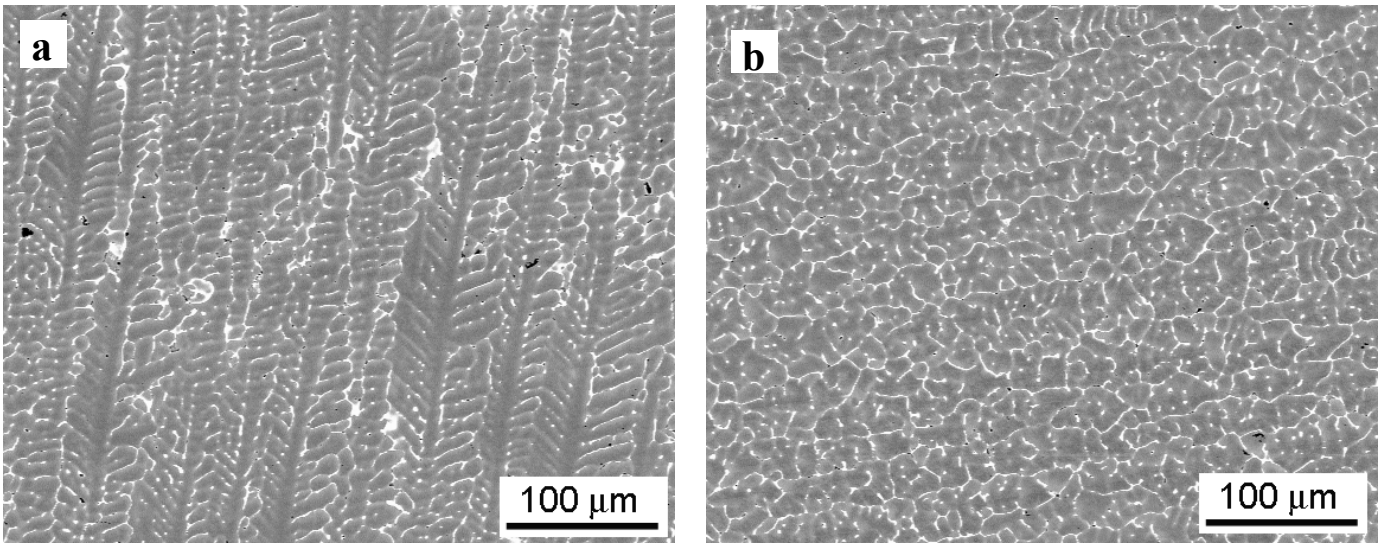

Figure 2. SEM backscatter micrographs of (a) longitudinal and (b) transverse cross-sections of the DC cast ingot of alloy SSA000.

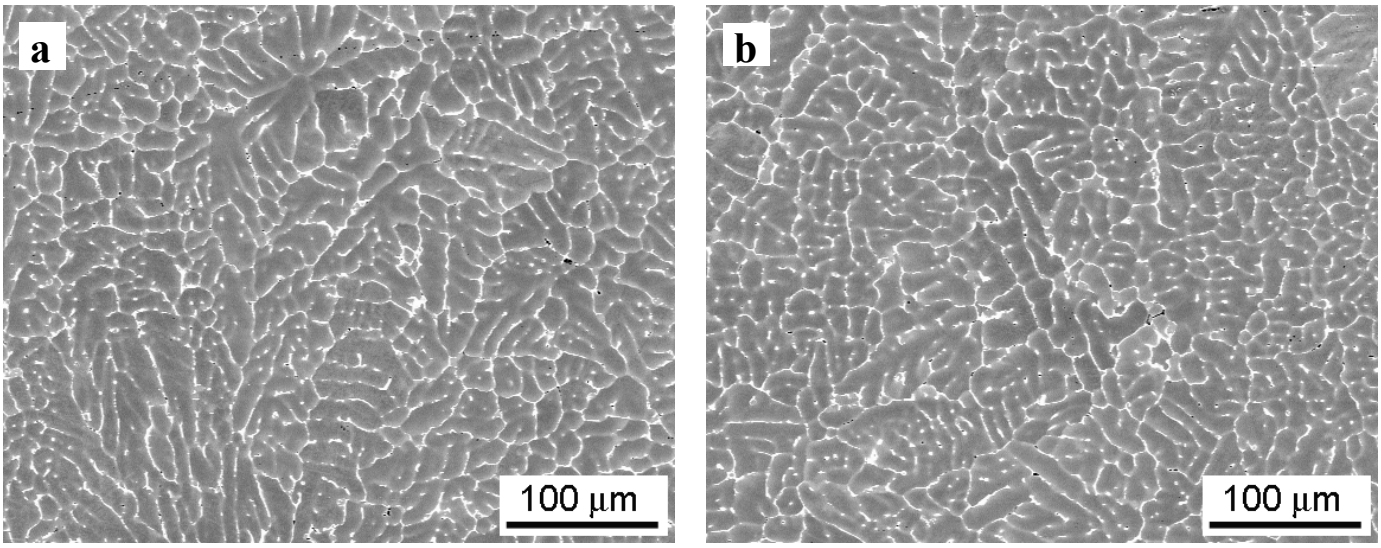

Figure 3. SEM backscatter micrographs of (a) longitudinal and (b) transverse cross-sections of the DC cast ingot of alloy SSA018.

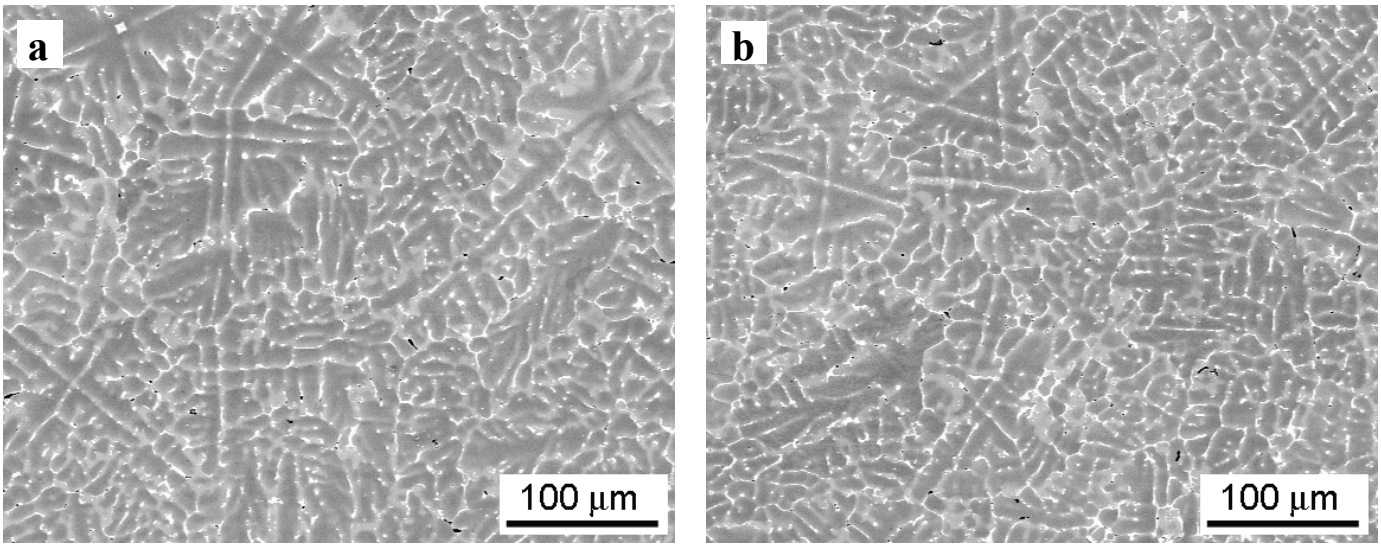

Figure 4. SEM backscatter micrographs of (a) longitudinal and (b) transverse cross-sections of the DC cast ingot of alloy SSA038.

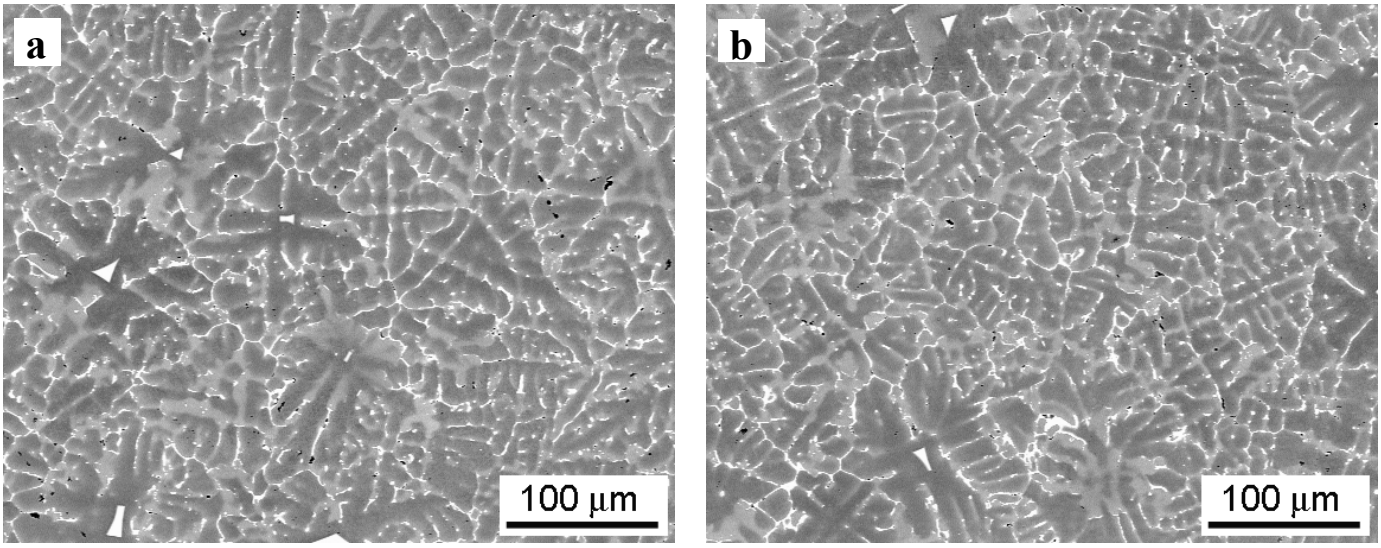

Figure 5. SEM backscatter micrographs of (a) longitudinal and (b) transverse cross-sections of the DC cast ingot of alloy SSA048.

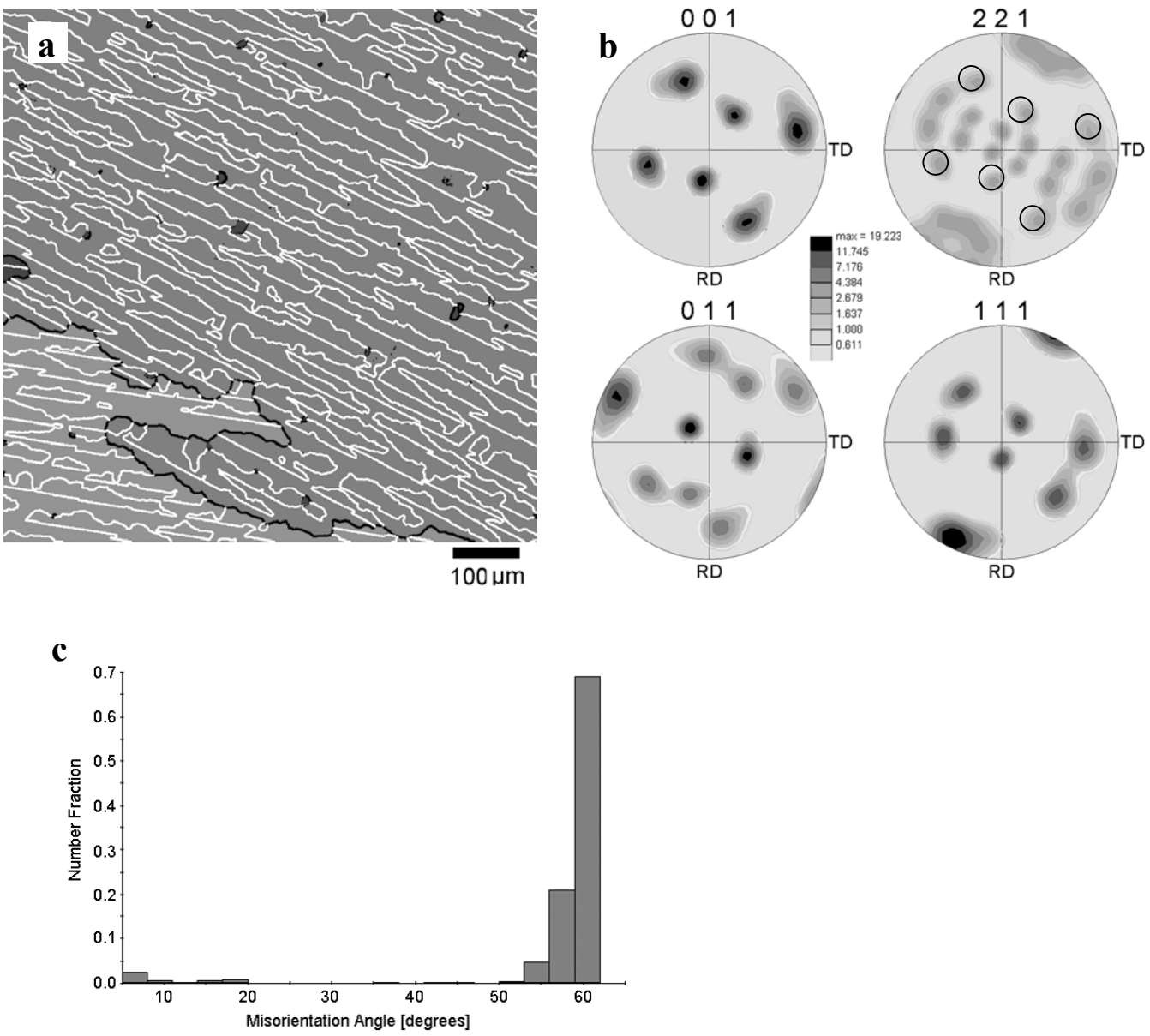

Figure 6. Orientation imaging microscopy (OIM) data of alloy SSA000 showing (a) the grain structure, (b) characteristic pole figures and (c) the misorientation angle distribution between the adjacent grains. In figure (a), the boundaries between the matrix and twins are highlighted with white lines, and the boundaries between the matrix grains are highlighted with black lines. In figure (b) <221> poles from twins and the matrix, which are parallel to <001> poles from the matrix and twins, respectively, are circled.

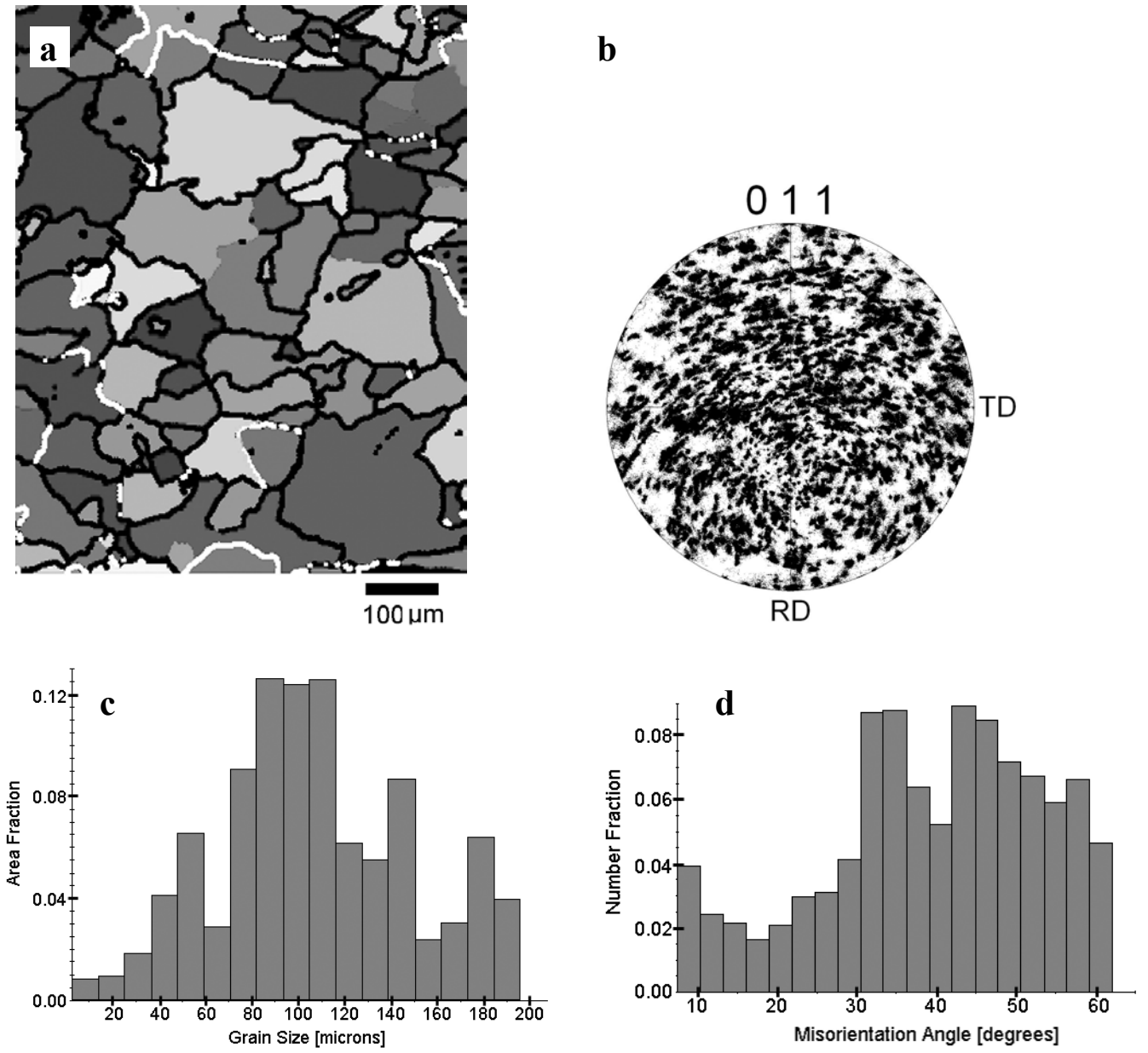

Figure 7. Orientation imaging microscopy (OIM) data of alloy SSA018 showing (a) the grain structure, (b) the (011) discrete pole figure showing orientations of all individual grains, (c) the grain size distribution plot and (d) the distribution of the misorientation angle between the adjacent grains. In figure (a), the boundaries between the twin-oriented crystals are highlighted with white lines, and other boundaries are highlighted with black lines.

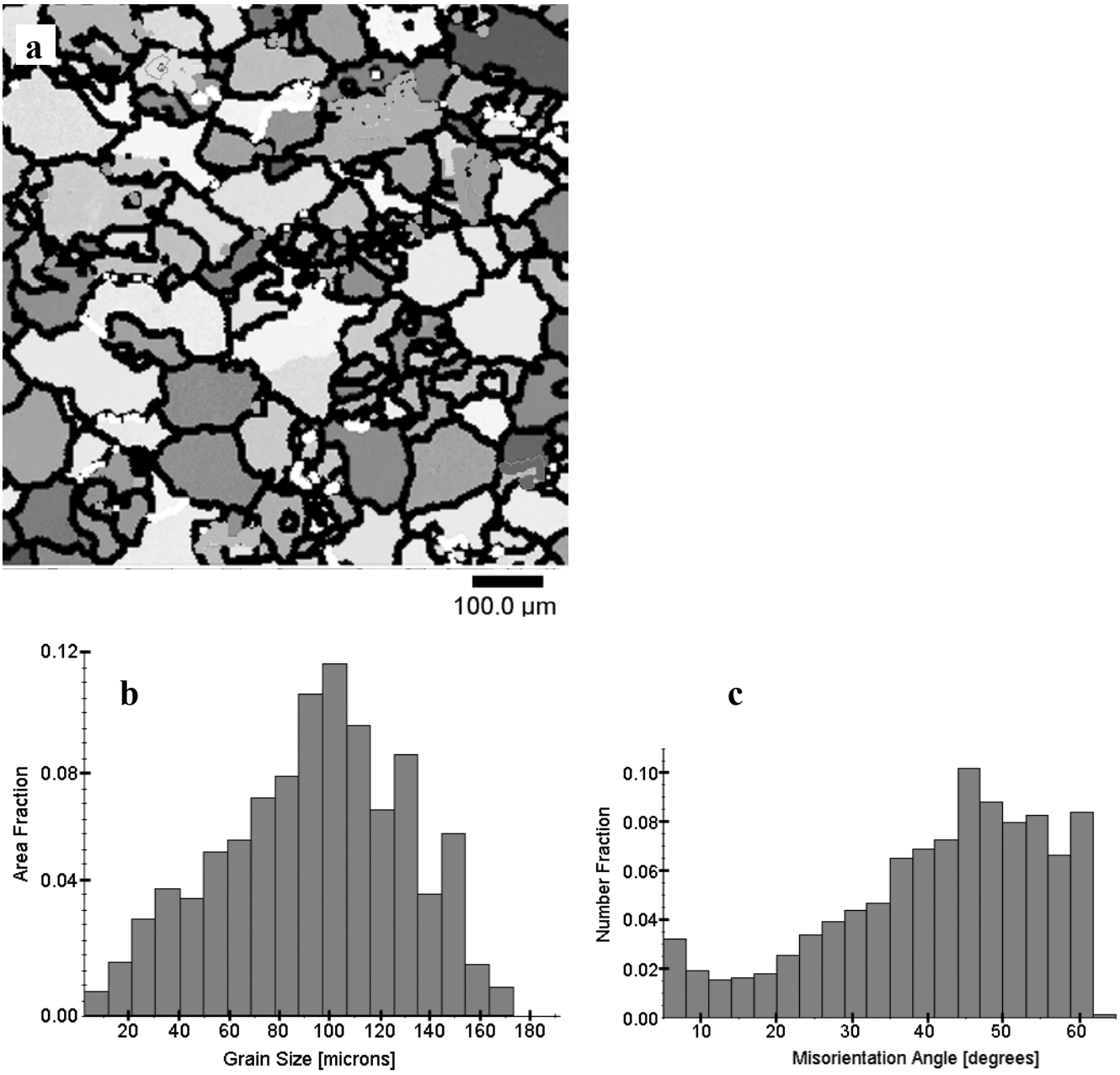

Figure 8. Orientation imaging microscopy (OIM) data of alloy SSA048 showing (a) the grain structure, (b) the grain size distribution plot and (c) the distribution of the misorientation angle between the adjacent grains.

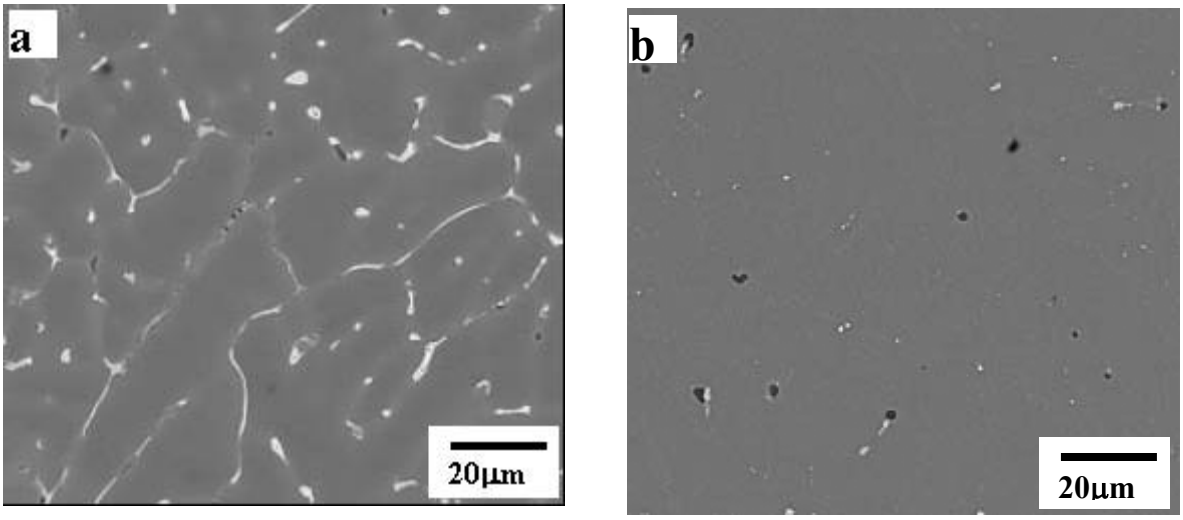

Figure 9. SEM BSE micrographs of SSA018 showing (a) as-cast and (b) as-homogenized structure.

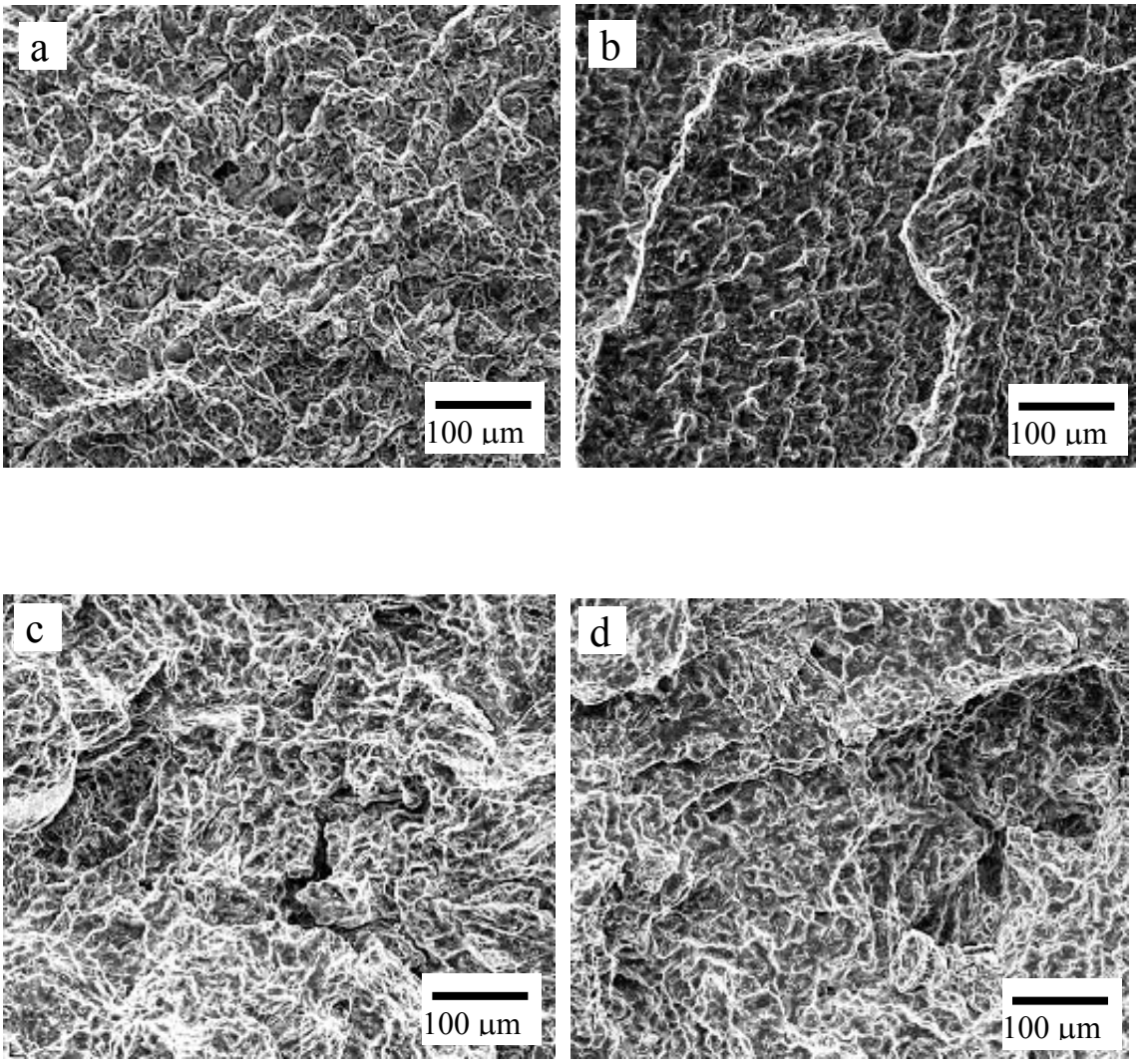

Figure 10. SEM fractographs of tensile specimens of the alloys SSA000 (a and b) and SSA018 (c and d), with the tensile axis in the longitudinal (a, c) and transverse (b, d) directions. H+T6 condition, room temperature deformation.

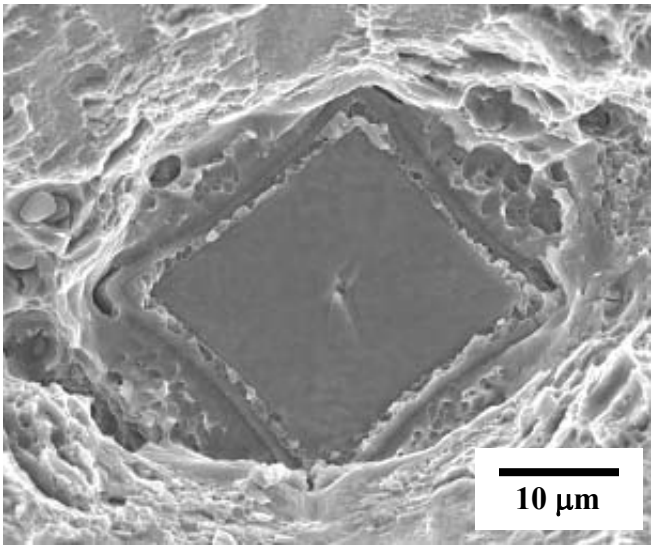

Figure 11. SEM fractograph from the alloy SSA048 showing cleavage fracture of a coarse primary $Al_3(Sc,Zr)$ particle.